

1

[ATLAS Semivisible Jets]

2

[Elena Laura Busch]

3

Submitted in partial fulfillment of the  
requirements for the degree of  
Doctor of Philosophy  
under the Executive Committee  
of the Graduate School of Arts and Sciences

4

5

6

7

8

COLUMBIA UNIVERSITY

9

2024

10

© 2024

11

[Elena Laura Busch]

12

All Rights Reserved

13

## **Abstract**

14

[ATLAS Semivisible Jets]

15

[Elena Laura Busch]

16

Abstract of dissertation (place-holder).

## Table of Contents

|    |  |    |
|----|--|----|
| 18 | Acknowledgments . . . . .                      | v  |
| 19 | Dedication . . . . .                           | vi |
| 20 | Introduction or Preface . . . . .              | 1  |
| 21 | Chapter 1: The Standard Model . . . . .        | 2  |
| 22 | Chapter 2: The Large Hadron Collider . . . . . | 4  |
| 23 | 2.1 LHC Timeline . . . . .                     | 4  |
| 24 | 2.2 Accelerator Physics . . . . .              | 5  |
| 25 | 2.2.1 The Journey of a Proton . . . . .        | 5  |
| 26 | 2.2.2 Magnets . . . . .                        | 7  |
| 27 | 2.3 Luminosity . . . . .                       | 8  |
| 28 | Chapter 3: The ATLAS Detector . . . . .        | 10 |
| 29 | 3.1 Coordinate System and Geometry . . . . .   | 10 |
| 30 | 3.2 Inner Detector . . . . .                   | 12 |
| 31 | 3.2.1 Pixel Detector . . . . .                 | 12 |
| 32 | 3.2.2 Semiconductor Tracker . . . . .          | 13 |
| 33 | 3.2.3 Transition Radiation Tracker . . . . .   | 13 |

|    |  |    |
|----|--|----|
| 34 | 3.3 Calorimeters . . . . .                   | 14 |
| 35 | 3.3.1 Liquid Argon Calorimeter . . . . .     | 15 |
| 36 | 3.3.2 Tile Calorimeter . . . . .             | 18 |
| 37 | 3.4 Muon Spectrometer . . . . .              | 19 |
| 38 | 3.5 Magnet System . . . . .                  | 21 |
| 39 | 3.6 Forward Detectors . . . . .              | 22 |
| 40 | Conclusion or Epilogue . . . . .             | 24 |
| 41 | References . . . . .                         | 28 |
| 42 | Appendix A: Experimental Equipment . . . . . | 30 |
| 43 | Appendix B: Data Processing . . . . .        | 31 |

## List of Figures

|    |  |    |
|----|--|----|
| 45 | 2.1 Timeline of LHC activities [9] . . . . .   | 5  |
| 46 | 2.2 The LHC accelerator complex at CERN [11] . . . . .   | 6  |
| 47 | 2.3 The octants of the LHC and location of various beam activities [10] . . . . .                    | 8  |
| 48 | 3.1 ATLAS coordinate system and geometry . . . . .   | 12 |
| 49 | 3.2 A 3D visualization of the structure of the ID in the barrel region [13] . . . . .                | 13 |
| 50 | 3.3 ATLAS calorimetery system [14] . . . . .   | 14 |
| 51 | 3.4 Diagram of a segment of the EMB, demonstrating the accordion plate arrangement<br>[15] . . . . . | 16 |
| 53 | 3.5 A LAr pulse as produced in the detector (triangle) and after shaping (curve) [15] . .            | 17 |
| 54 | 3.6 Readout gap structure in HEC [15] . . . . .  | 17 |
| 55 | 3.7 TileCal wedge module [18] . . . . .  | 19 |
| 56 | 3.8 Cross section view of the muon spectrometer system [19] . . . . .                                | 20 |
| 57 | 3.9 Layout of the barrel and endcap toroid magnets [22] . . . . .                                    | 22 |

## **List of Tables**

59

## Acknowledgements

60        Insert your acknowledgements text here. This page is optional, you may delete it if not  
61        needed.

62

## **Dedication**

63

Dedicated to my friends and family

64

## **Introduction or Preface**

65        Insert your preface text here if applicable. This page is optional, you may delete it if not  
66    needed. If you delete this page make sure to move page counter comment in thesis.tex to correct  
67    location.

68

## 69 Chapter 1: The Standard Model

70 Four fundamental forces

71 The Standard Model is a universally accepted framework which explains most of the interactions  
72 of fundamental particles. The SM is a renormalizable quantum field theory that obeys the local symmetry  $G_{SM}$ :

$$G_{SM} = SU(3)_C \times SU(2)_L \times U(1)_Y \quad (1.1)$$

74 The  $SU(3)_C$  symmetry component is the non-Abelian gauge group of quantum chromodynamics (QCD), the theory of strong interactions. There are 8 generators for the  $SU_C(3)$  group which correspond to *gluons*, massless spin-1 gauge boson which carry the force of the strong interaction.

77 Gluon and quarks, the particles which interact with the strong force, carry a color charge  $C$ .

78 The  $SU(2)_L \times U(1)_Y$  symmetry group represents the electroweak sector of the Standard Model.  
79 There are 4 generators for this group, which correspond to the four massless gauge bosons  $W^1$ ,  $W^2$ ,  
80  $W^3$ , and B. From these massless gauge bosons are formed the massive mediators of the weak force,  
81 the  $W^-$ ,  $W^+$  and  $Z^0$  bosons, and the massless electromagnetic force carrier, the photon  $\gamma$ .

82 The interplay between the fermionic and bosonic fields that emerge from the  $G_{SM}$  symmetry  
83 can be described through the Lagrangian in equation 1.2

$$\mathcal{L} = \mathcal{L}_{kin} + \mathcal{L}_\psi + \mathcal{L}_{Yuk} + \mathcal{L}_\phi \quad (1.2)$$

84 Each term in this Lagrangian describes a set of specific particle physics interactions.  $\mathcal{L}_{kin}$   
85 . with three families of quarks and leptons, and a scalar Higgs doublet. The standard model  
86 has 12 gauge bosons: 8 gluons, 3 weak bosons, and the photon. [1]

87 The physics of the Standard Model of particle physics (SM) is summarized by the SM La-  
88 grangian:

$$\mathcal{L}_{kin} = -\frac{1}{4}F_{\mu\nu}F^{\mu\nu} \quad (1.3)$$

- 89 Explain equation
- 90 Explain phenomonolyg

91

92

## Chapter 2: The Large Hadron Collider

93       The Large Hadron Collider (LHC) is a 26.7km circular high-energy particle accelerator, span-  
94       ning the Swiss-French border near the city of Geneva, Switzerland [2]. The LHC occupies the  
95       tunnel constructed in 1989 for the Large Electron-Positron (LEP) Collider, and reaches a maxi-  
96       mum depth of 170m below the surface. The LHC is operated by the European Organization for  
97       Nuclear Research (CERN), the largest international scientific collaboration in the world.

98

99       The LHC accelerates protons and heavy ions and collides them at four interaction points around  
100      the ring, with a design center-of-mass energy per collision of  $\sqrt{s} = 14$  TeV. Each interaction point  
101      is home to one of four detector experiments, which study the products of the collisions. The largest  
102      of these experiments is the ATLAS detector, a general purpose detector designed to study the Stan-  
103      dard Model and search for new physics that could be produced in LHC collisions [3]. The CMS  
104      detector is another general purpose detector, designed and operated independently of the ATLAS  
105      detector, but intended to probe the same range of physics [4]. The ALICE experiment is a dedi-  
106      cated heavy ion experiment, and the LHC-b experiment is a dedicated *b*-physics experiment [5] [6].

107

### 108     **2.1 LHC Timeline**

109       The first proton-proton collisions at the LHC were achieved in 2010 with a center-of-mass  
110      energy of  $\sqrt{s} = 7$  TeV. Run 1 of the LHC took place between 2010 and 2013. The data collected  
111      during this time led to the discovery of the Higgs Boson in 2012 [7]. Between 2013 and 2015  
112      the LHC underwent the first Long Shutdown (LS1) during which time key upgrades to the physics  
113      detectors and the accelerator chain were installed. Run 2 of the LHC took place from 2015 to 2018



Figure 2.1: Timeline of LHC activities [9]

and achieved a center-of-mass energy of  $\sqrt{s} = 13$  TeV. Between 2018 and 2022 the LHC underwent its second Long Shutdown (LS2). Run-3 of the LHC began in 2022 and achieved a center-of-mass energy of  $\sqrt{s} = 13.6$  TeV. Run-3 is scheduled to continue through 2026, at which point the LHC machine and detectors will undergo upgrades for the *high luminosity* LHC (HL-LHC), which will increase the number of collisions by a factor of 5-10 with respect to the nominal LHC design [8].

## 2.2 Accelerator Physics

### 2.2.1 The Journey of a Proton

Protons which feed the LHC start as hydrogen gas. The electrons are removed from the hydrogen atoms through the use of strong electric fields. The linear accelerator (LINAC) then accelerates the  $H^-$  ions to an energy of 50 MeV. From here the  $H^-$  ions enter the Proton Synchrotron booster, where they are accelerated up to 1.4 GeV of energy. Subsequently they are sorted into bunches separated in time by 25 ns, where each bunch contains approximately  $10^{11}$  protons. Next the bunches pass through the Proton Synchrotron (PS) and the Super Proton Synchrotron (SPS), where they reach energies of 25 GeV and 450 GeV respectively. Finally they are injected into the LHC as two

## The CERN accelerator complex *Complexe des accélérateurs du CERN*

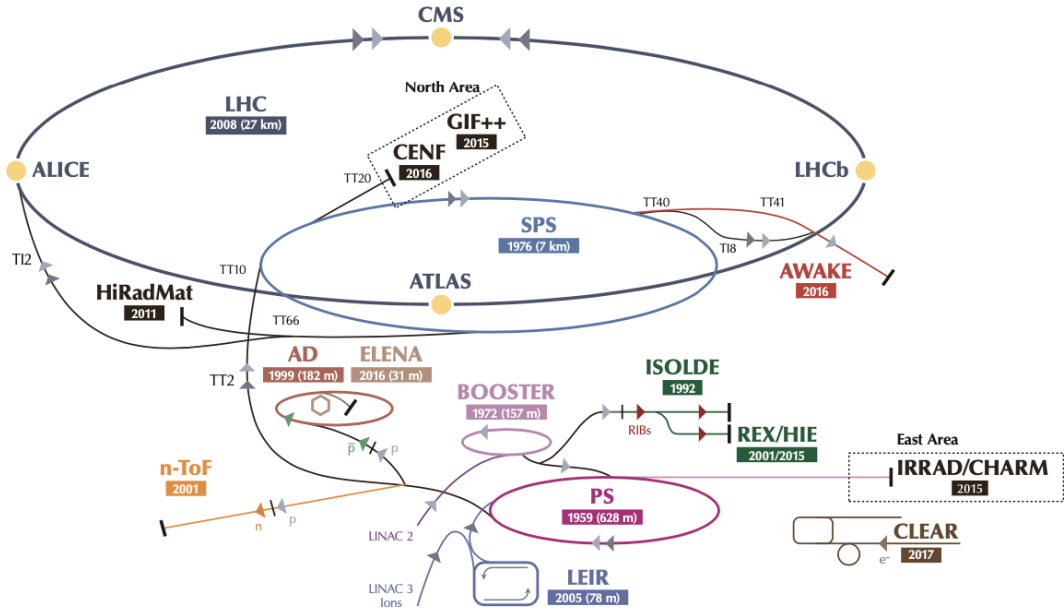


Figure 2.2: The LHC accelerator complex at CERN [11]

129 beams traveling in opposite direction. The original design allowed each beam to be accelerated  
 130 up to 7 TeV of energy. Due to limitations with the magnet training, the highest energy actually  
 131 achieved by the LHC beams during Run 2 was 6.5 TeV, giving a collision center-of-mass energy  
 132 of  $\sqrt{s} = 13$  TeV [10]. Figure 2.2 shows the full LHC accelerator complex.

133

134 Acceleration in the LHC is performed by eight radio frequency (RF) cavities located around the  
 135 ring. Each RF cavity produces a 2MV electric field oscillating at 40 MHz. The 40MHz oscillation  
 136 produces a point of stable equilibrium every 2.5ns. These points of equilibrium are synchronized  
 137 with the occurrence of the proton bunches produced in the PS – a proton bunch occupies one out  
 138 of every ten points of stable equilibrium, such that the bunches maintain a 25ns spacing [10].

139

140 2.2.2 Magnets

141 In addition to the acceleration cavities, the LHC houses 9593 superconducting magnets which  
142 direct and focus the proton beam on its 27 kilometer journey. The magnets are comprised of super-  
143 conducting Niobium-Titanium coils cooled to 1.9K by superfluid helium. As the beams approach  
144 one of the four collision points around the ring, multipole magnets focus and squeeze the beam for  
145 optimal collisions [10].

146 The LHC is divided into sections, where each section contains an a smoothly curving *arc* and  
147 a straight *insertion*. The arcs are composed of 1232 large dipole magnets which bend the beam  
148 to follow the roughly circular 27 km path. The main dipoles generate powerful 8.3 tesla magnetic  
149 fields to achieve this bend. Each dipole magnet is 15 meters long and weighs 35 tonnes. The  
150 dipoles work in conjunction with quadrupole magnets, which keep the particles in a focused beam,  
151 and smaller sextupole, octupole and decapole magnets which tune the magnetic field at the ends of  
152 the dipole magnets [12].

153 The straight insertion sections have different purposes depending on their location around the  
154 ring: beam collisions, beam injection, beam dumping, or beam cleaning. At the four collision  
155 points, insertion magnets squeeze the beam to ensure a highly focused collision. This is accom-  
156 plished with a triplet of quadrupole magnets, which tighten the beam from 0.2 millimeters to just  
157 16 micrometers in diameter. Insertion magnets also clean the beam, which prevents stray particles  
158 from hitting sensitive components throughout the LHC. When the LHC is ready to dispose of a  
159 beam of particles, beam dump magnets deflect the path of the beam into a straight line towards  
160 a block of concrete and graphite that stops the beam. A dilution magnet then reduces the beam  
161 intensity by a factor of 100,000 before the final stop [12]. Figure 2.3 shows the locations various  
162 beam activities.

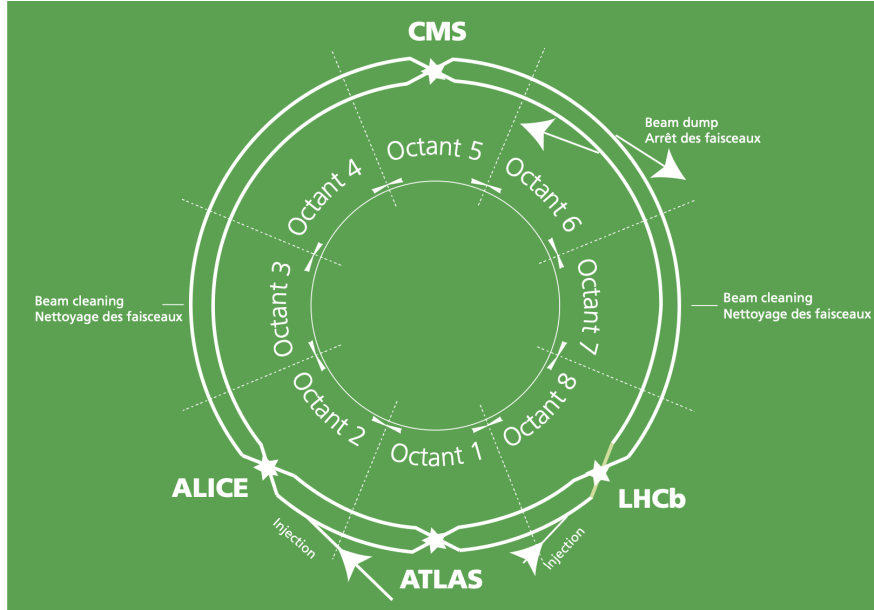


Figure 2.3: The octants of the LHC and location of various beam activities [10]

### <sup>163</sup> 2.3 Luminosity

<sup>164</sup> Collisions at the LHC occur when the two beams of proton bunches cross at one of the four  
<sup>165</sup> interaction points. The intensity of collisions is described by the instantaneous luminosity, the  
<sup>166</sup> formula for which is given in equation 2.1.

$$L = \frac{f N_1 N_2}{4\pi \sigma_x \sigma_y} \quad (2.1)$$

<sup>167</sup> Here  $f$  is the revolution frequency,  $N_1$  and  $N_2$  are the number of particle per bunch for each  
<sup>168</sup> beam, and  $\sigma_x$ ,  $\sigma_y$  are the horizontal and vertical beam widths.

<sup>169</sup>

<sup>170</sup> The instantaneous luminosity gives the number of the collisions that could be produced at the  
<sup>171</sup> interaction point per  $\text{cm}^2$  of cross-sectional area per second. The integrated luminosity is obtained  
<sup>172</sup> by integrating the instantaneous luminosity over a given block of time, and measures the total num-  
<sup>173</sup> ber of collisions which has occurred during that operation period. This is directly correlated with  
<sup>174</sup> the size of the datasets collected by the LHC experiments.

175

176     The design peak luminosity of the LHC is  $1.0 \times 10^{34} \text{ cm}^{-2}\text{s}^{-1}$ . During Run 1 of the LHC the  
177     peak instantaneous luminosity was  $0.8 \times 10^{34} \text{ cm}^{-2}\text{s}^{-1}$ . Over the course of Run 1 the LHC collected  
178     a total integrated luminosity of  $5.46 \text{ fb}^{-1}$  at  $\sqrt{s} = 7 \text{ TeV}$ , and  $22.8 \text{ fb}^{-1}$  at  $\sqrt{s} = 8 \text{ TeV}$ . Following the  
179     first long shutdown and upgrade phase of operations, the LHC achieved a center of mass energy  
180      $\sqrt{s} = 13 \text{ TeV}$  at the beginning of Run 2 in 2015. The LHC was also able to deliver  $2.0 \times 10^{34}$   
181      $\text{cm}^{-2}\text{s}^{-1}$  peak instantaneous luminosity, double the design value. During LHC Run 2, from 2015-  
182     2018, the LHC delivered  $156 \text{ fb}^{-1}$  of integrated luminosity for proton-proton collisions. Run 3 of  
183     the LHC began in 2022, and is expected to deliver  $250 \text{ fb}^{-1}$  of integrated luminosity to the ATLAS  
184     and CMS experiments by 2026 [9].

185

186     The goal of LHC physic analyses is to find and study rare events produced by interesting  
187     physics processes. The cross section  $\sigma$  of a given process indicates the probability of that process  
188     occurring given the beam conditions of the LHC. Multiplying the cross section by the integrated  
189     luminosity of a dataset gives the expected number of events for that process within the dataset.

$$N_{\text{events}} = \int \sigma L(t) dt = \mathcal{L} \times \sigma \quad (2.2)$$

190     The cross section for most processes of interest, especially BSM processes, is several orders of  
191     magnitude below the total cross section for the LHC. Therefore maximizing the number of events  
192     produced in collisions is crucial to increase the likelihood of producing events from processes of  
193     interest. For this reason, maximizing instantaneous luminosity is a key factor in accelerator design  
194     and operation.

195

196

## Chapter 3: The ATLAS Detector

197     The ATLAS detector is one of two general purpose physics detectors designed to study the  
198   products of the proton-proton collisions produced by the LHC. The detectors is composed of a  
199   variety of specialized subsystems, designed to fully capture the large array of physics processes  
200   produced in the LHC. The apparatus is 25m high, 44m in length, and weighs over 7000 tons. Colli-  
201   sions occur directly in the center of the apparatus, and the cylindrical design of the detector allows  
202   a complete 360 view of any physics objects resulting from the collision to be reconstructed.

203

204     Two magnet systems provide strong magnetic fields, which bend the trajectory of charged  
205   particles as they pass through the magnetic fields; this allows the calculation of the momentum  
206   of the particles. A 2T solenoid magnet provides a uniform magnetic field to the inner layers of  
207   the detector. Further out, a toroidal magnet system ( TODO: how many toroids?) provides fields  
208   strengths of 0.5 to 1T

### 209   **3.1 Coordinate System and Geometry**

210     The ATLAS detector employs a right hand cylindrical coordinate system. The  $z$  axis is aligned  
211   with the beam line, and the x-y plane sits perpendicular to the beam line. The origin is centered on  
212   the detector, such that the origin corresponds with the interaction point of the two colliding beams.  
213     The detector geometry is usually characterized by polar coordinates, where the azimuthal angle  $\phi$   
214   spans the x-y plane. The polar angle  $\theta$  represents the angle away from the beam line, or  $z$  axis.  
215      $\theta = 0$  aligns with the positive  $z$ -axis, and  $\phi = 0$  aligns with the positive x-axis.

216

217     The polar coordinate  $\theta$  is generally replaced by the Lorentz invariant quantity *rapidity*  $y$ .

$$y = \frac{1}{2} \ln\left(\frac{E + p_z}{E - p_z}\right) \quad (3.1)$$

218 This substitution is advantageous because objects in the detector are traveling at highly rela-  
 219 tivistic speeds. The relativistic speed of objects passing through the ATLAS detector also means  
 220 that the masses of the particles are generally small compared to their total energy. In the limit of  
 221 zero mass, the rapidity  $y$  reduces to the *pseudorapidity*  $\eta$ , which can be calculated directly from  
 222 the polar angle  $\theta$ .

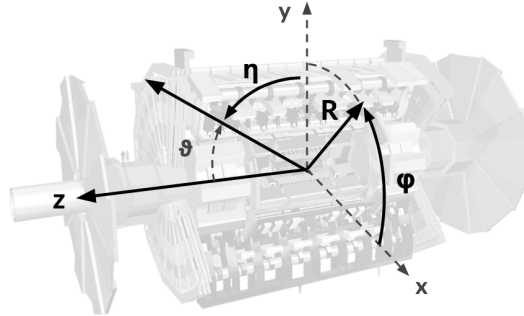
$$\eta = -\ln\left(\frac{\theta}{2}\right) \quad (3.2)$$

223 Figure 3.1a depicts the orientation of the coordinate system with respect to the ATLAS de-  
 224 tector, while Figure 3.1b illustrates the relationship between  $\theta$ ,  $\eta$ , and the beamline axis  $z$ . The  
 225 distance between physics objects in the detector is generally expressed in terms of the solid angle  
 226 between them  $\Delta R$ .

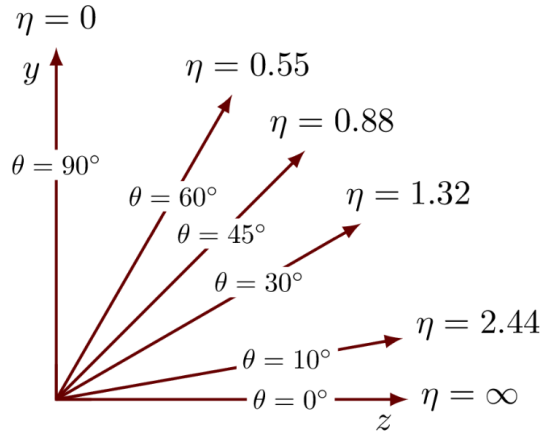
227

$$\Delta R = \sqrt{\Delta\phi^2 + \Delta\eta^2} \quad (3.3)$$

228 Head on proton-proton collisions are more likely to result in objects with a lot of energy in the  
 229 transverse plane; glancing proton-proton collisions are more likely to result in objects where most  
 230 of the energy is directed along the  $z$ -axis. Due to the importance of categorizing these objects,  
 231 as well as the cylindrical design of the ATLAS detector, the detector is generally divided  
 232 into regions in  $\eta$ . Each subsystem has a “central” or “barrel” region covering low  $|\eta|$ , while the  
 233 “forward” or “endcap” regions cover  $|\eta|$  up to 4.9. Each of the three main ATLAS subsystems will  
 234 be discussed in the following sections.



(a) The ATLAS geometry



(b) Relationship between  $\eta$  and  $\theta$

Figure 3.1: ATLAS coordinate system and geometry

## 235 3.2 Inner Detector

236 The Inner Detector (ID) is the ATLAS subsystem closest to the interaction point. The primary  
 237 purpose of the ID is to determine the charge, momentum, and trajectory of charged particles pass-  
 238 ing through the detector. With this information the ID is also able to precisely determine interaction  
 239 vertices.

240

241 The ID is composed of three sub-detectors; the pixel detector, the semiconductor tracker (SCT)  
 242 and the transition radiation tracker (TRT). Figure 3.2 shows the location of these three subsystems  
 243 with respect to each other and the interaction point.

### 244 3.2.1 Pixel Detector

245 The pixel detector is the first detector encountered by particles produced in LHC collisions.  
 246 The original pixel detector consists of 3 barrel layers of silicon pixels, positioned at 4cm, 11cm  
 247 and 14cm from the beamline. There are also 4 disks on each side positioned between 11 and 20cm,  
 248 providing full coverage  $|\eta| < 2.5$ . The layers are comprised of silicon pixels each measuring 50  
 249  $\mu\text{m}$  by  $300 \mu\text{m}$ , with 140 million pixels in total. The pixels are organized into modules, which  
 250 each contain a set of radiation hard readout electronics chips. In 2014, the Insertable B-layer

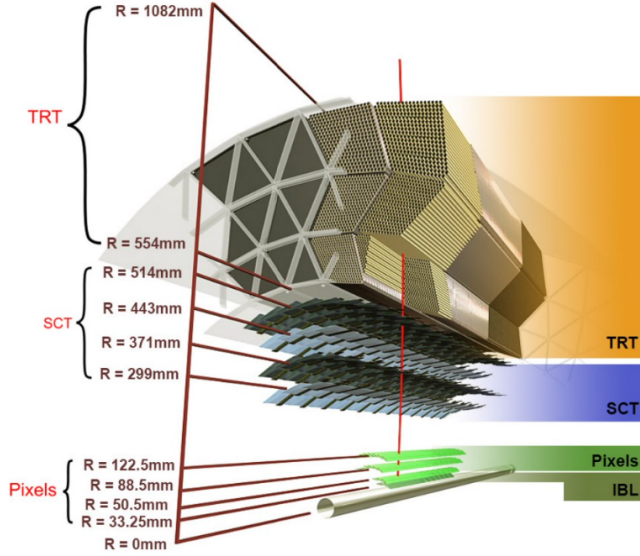


Figure 3.2: A 3D visualization of the structure of the ID in the barrel region [13]

(IBL) was installed, creating a new innermost layer of the pixel detector sitting just 3.3cm from the beamline. The pixels of the IBL measure  $50 \mu\text{m}$  by  $250 \mu\text{m}$ , and cover a pseudo-rapidity range up to  $|\eta| < 3$ . The IBL upgrade enhances the pixel detector's ability to reconstruct secondary vertices associated with short-lived particles such as the b-quark. The improved vertex identification also helped compensate for increasing pile-up in Run 2.

### 3.2.2 Semiconductor Tracker

The SCT provides at least 4 additional measurements of each charged particle. It employs the same silicon technology as the Pixel Detector, but utilizes larger silicon strips which measure  $80\mu\text{m}$  by 12.4cm. The SCT is composed of 4 barrel layers, located between 30cm and 52cm from the beamline, and 9 end-cap layers on each side. The SCT can distinguish tracks that are separated by at least  $200\mu\text{m}$ .

### 3.2.3 Transition Radiation Tracker

The TRT provides an additional 36 hits per particle track. The detector relies on gas filled straw tubes, a technology which is intrinsically radiation hard. The straws which are each 4mm in

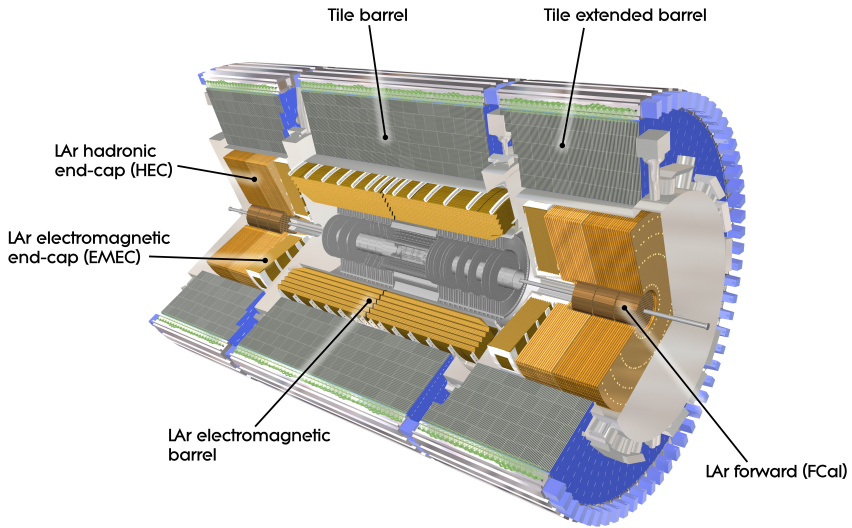


Figure 3.3: ATLAS calorimetry system [14]

265 diameter and up to 150cm in length and filled with xenon gas. The detector is composed of about  
 266 50000 barrel region straws and 640000 end-cap straws, comprising 420000 electronic readout  
 267 channels. Each channel provides a drift time measurement with a spatial resolution of  $170\mu\text{m}$   
 268 per straw. As charged particles pass through the detector and interact with the xenon, transition  
 269 radiation is emitted. The use of two different drift time thresholds allows the detector to distinguish  
 270 between tracking hits and transition radiation hits.

271 **3.3 Calorimeters**

272 The ATLAS calorimeter system is responsible for measuring the energy of electromagnetically  
 273 and hadronically interacting particles passing through the detector. The calorimeters are located  
 274 just outside the central solenoid magnet, which encloses the inner detectors. The calorimeters also  
 275 stop most known particles, with the exception of muons and neutrinos, preventing them from  
 276 traveling to the outermost layers of the detector. The ATLAS calorimetry system is composed of  
 277 two subsystems - the Liquid Argon (LAr) calorimeter for electromagnetic calorimetry and the Tile  
 278 calorimeter for hadronic calorimetry. The full calorimetry system is shown in figure 3.3.

279 3.3.1 Liquid Argon Calorimeter

280 The LAr calorimeter is a sampling calorimeter designed to trigger on and measure the energies  
281 of electromagnetic particles, as well as hadronic particles in the high  $\eta$  regions. It is divided in sev-  
282 eral regions, as shown in Figure 3.3. For the region  $|\eta| < 1.4$ , the electromagnetic barrel (EMB) is  
283 responsible for electronic calorimetery, and provides high resolution energy, timing, and position  
284 measurements for electrons and photons passing through the detector. The electromagnetic endcap  
285 (EMEC) provides additional EM calorimetery up to  $|\eta| < 3.2$ . In the region  $1.4 < |\eta| < 3.2$ , the  
286 hadronic endcap (HEC) provides hadronic calorimetery. For hadronic calorimetery In the region  
287  $|\eta| < 1.4$ , corresponding to a detector radii  $> 2.2\text{m}$ , the less expensive tile calorimeter (discussed  
288 in the next section) is used instead. A forward calorimeter (FCAL) extends the hadronic calorime-  
289 tery coverage up to  $3.1 < |\eta| = 4.8$  [15].

290

291 The LAr calorimeter is composed of liquid argon sandwiched between layers of absorber mate-  
292 rial and electrodes. Liquid argon is advantageous as a calorimeter active medium due to its natural  
293 abundance and low cost, chemical stability, radiation tolerance, and linear response over a large  
294 energy range [16]. The calorimeter is cooled to 87k by three cryostats: one barrel cryostat encom-  
295 passing the EMB, and two endcap cryostats. The barrel cryostat also encloses the solenoid which  
296 produces the 2T magnetic field for the inner detector. Front end electronics are housed outside the  
297 cryostats and are used to process, store and transfer the calorimeter signals.

298

299 **Electromagnetic Calorimeter**

300 For the electromagnetic calorimeters, the layers of electrodes and absorber materials are ar-  
301 ranged in an an accordion shape, as illustrated in Figure 3.4. The accordion shape ensures that  
302 each half barrel is continuous in the azimuthal angle, which is a key feature for ensuring consistent  
303 high resolution measurements. Liquid argon permeates the space between the lead absorber plates,  
304 and a multilayer copper-polymide readout board runs through the center of the liquid argon filled

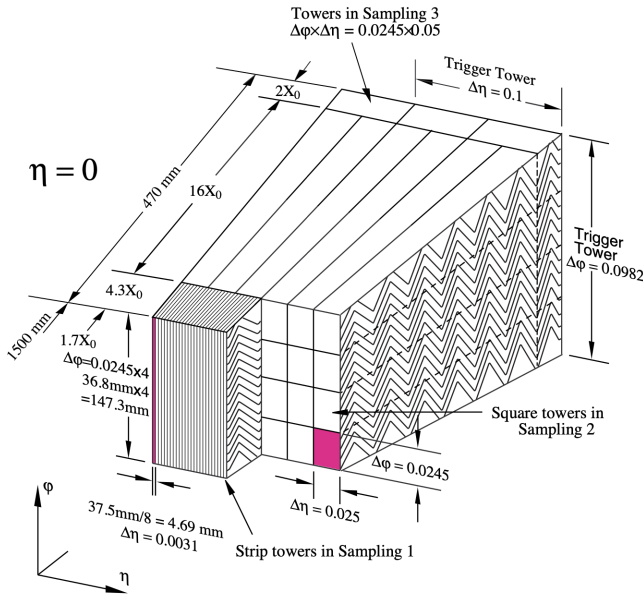


Figure 3.4: Diagram of a segment of the EMB, demonstrating the accordion plate arrangement [15]

305 gap.

306

307 The detection principle for the LAr calorimeter is the current created by electrons which are  
 308 released when a charged particle ionizes the liquid argon. In the barrel region, the electrons are  
 309 driven towards the center electrodes by a 2000V potential with a drift time of less than 450ns [17].

310 In the endcaps the voltage varies as a function of the radius in order to maintain a flat response [15].

311 The amount of current produced by the ionized electrons is proportional to the energy of the parti-  
 312 cle creating the signal. Figure ?? shows the shape of the signal produced in the LAr calorimeter,  
 313 before and after it undergoes shaping during the readout process. The shaping of the pulse enforces  
 314 a positive peak and a negative tail, which ensures that subsequent pulses can be separated with  
 315 the precision required for the 25ns LHC bunch spacing [15].

316

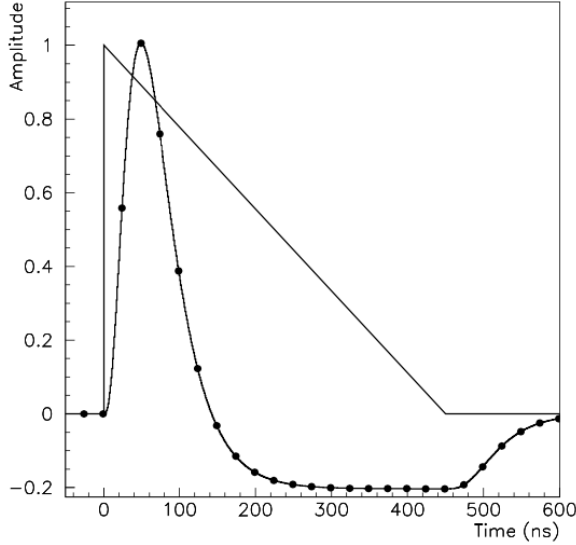


Figure 3.5: A LAr pulse as produced in the detector (triangle) and after shaping (curve) [15]

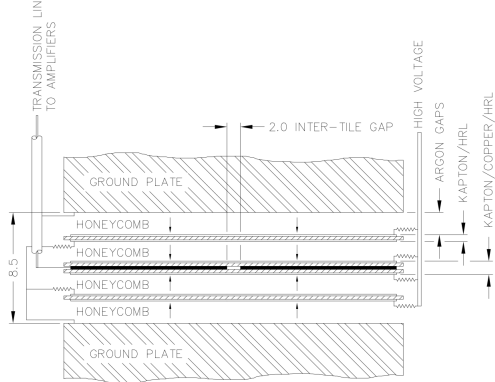


Figure 3.6: Readout gap structure in HEC [15]

### **Hadronic End-cap Calorimeter**

The HEC sits radially beyond the EMEC. The copper absorber plates in the HEC are oriented perpendicular to the beamline, with LAr as the active medium. Each end-cap is divided into two independent wheels; the inner wheel uses 25mm copper plates, while the outer wheel uses 50mm plates as a cost saving measure. In each wheel, the 8.5mm plate gap is crossed by three parallel electrodes, creating an effective drift distance of 1.8mm. This gap is illustrated in Figure 3.6. Each wheel is divided into 32 wedge-shaped modules, each containing their own set of readout electronics.

325    **Forward Calorimeter**

326    The forward range is covered by the FCAL, which provides both EM and hadronic calorimetry.  
327    It is composed of three active cylindrical modules; one EM module with copper absorber plates,  
328    and two hadronic modules with tungsten absorber plates. The plates are oriented perpendicular  
329    to the beamline, and LAr is used as the active material throughout. The electrodes of the FCal  
330    consist of tubes that run parallel to the beam line, arranged in a honeycomb pattern. The resulting  
331    LAr gaps are as small as  $250 \mu\text{m}$ , which enables the FCal to handle the high luminosities and the  
332    resulting large influx of particles in the forward region [15].

333    3.3.2 Tile Calorimeter

334    The tile calorimeter (TileCal) provides hadronic calorimetry in the region  $\eta < 1.7$ , and sur-  
335    rounds the LAr calorimeter. It is responsible for measurements of jet energy and jet substructure,  
336    and also plays an important role in electron isolation and triggering (including muons) [18]. Tile-  
337    Cal is composed of 3 sections, as shown in figure 3.3; a barrel calorimeter sits directly outside the  
338    LAr EMB and provides coverage up to  $\eta < 1.0$ . Two extended barrel sections sit outside the LAr  
339    endcaps and cover the region  $0.8 < \eta < 1.7$ .

340

341    TileCal is a sampling calorimeter composed of steel and plastic scintillator plates as illustrated  
342    in Figure 3.7. A total of 460,000 scintillators are read out by wavelength-shifting fibers. The  
343    fibers are gathered to define cells and in turn read out by photomultiplier tubes, which amplify  
344    the signal and convert it to an electrical signature. Each cell has an approximate granularity of  
345     $\Delta\eta \times \Delta\phi = 0.1 \times 0.1$ . Each barrel is divided azimuthally into 64 independent modules, an example  
346    of which is show in Figure 3.7. The modules are each serviced by front-end electronic housed in a  
347    water-cooled drawer on the exterior of the module.

348

349    The detection principle of the TileCal is the production of light from hadronic particles inter-  
350    acting with the scintillating tiles. When a hadronic particle hits the steel plate, a shower of particles

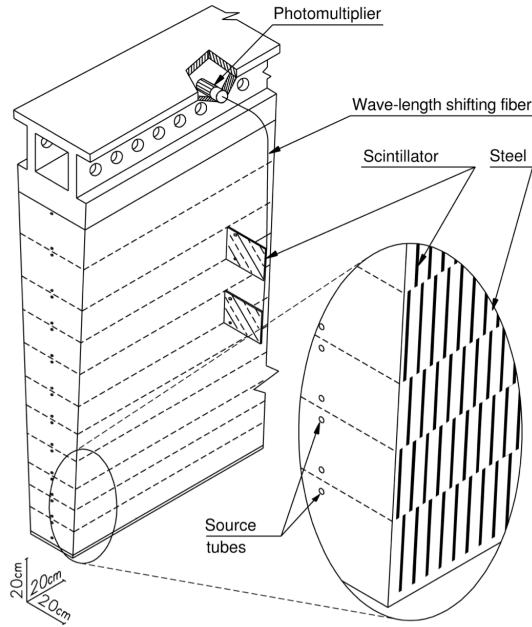


Figure 3.7: TileCal wedge module [18]

351 are produced. The interaction of the shower with the plastic scintillator produces photons, the num-  
 352 ber and intensity of which are proportional to the original particle's energy.

353

### 354 3.4 Muon Spectrometer

355 Unlike electrons, photons, and hadrons, muons interact minimally with the ATLAS calorime-  
 356 ters, and can pass through large amounts of detector material without stopping. The ATLAS muon  
 357 spectrometer (MS) provides additional tracking information to improve the identification and mea-  
 358 surement of muons. The MS comprises the outermost layers of the detector, and is interspersed  
 359 with toroid magnets (discussed in section 3.5), which provide a magnetic field of approximately  
 360 0.5T. The magnetic field bends the trajectory of the muons as they pass through the detector, and  
 361 the degree of the bend is directly correlated with the muon momentum. The path of the muon  
 362 is primarily measured by hits in three layers of monitored drift tube (MDT) precision chambers,  
 363 which cover the range  $|\eta| < 2.7$ . The barrel layout of the MS is show in Figure 3.8.

364

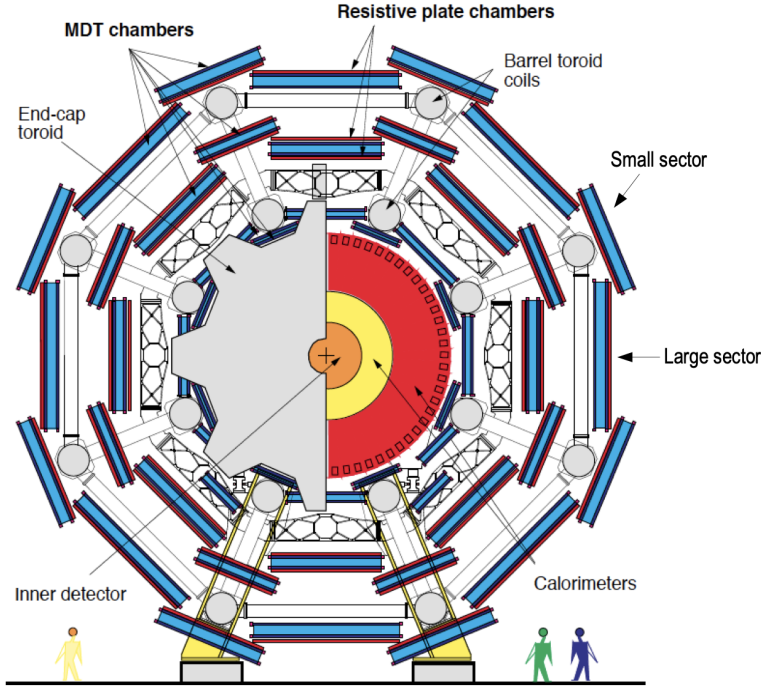


Figure 3.8: Cross section view of the muon spectrometer system [19]

365 Muon triggering is provided by three layers of resistive place chambers (RPC) in the barrel  
 366 ( $|\eta| < 1.05$ ), and 3-4 layers of thin gap chambers (TGC) in the endcaps ( $1.05 < |\eta| < 2.4$ ). RPCs  
 367 and TGCs also provide muon track measurements in the non-bending coordinate ( $\phi$ ). RPCs are  
 368 constructed from two parallel resistive plates separated by a 2mm gap filled with a sensitive gas  
 369 mixture. This provides a total of six independent measurements for each muon track, with a spatial  
 370 resolution of 1cm and a time resolution of 1ns. Time measurements from the RPCs are primarily  
 371 associated to hits in the MDT precision chambers to correct the bunch crossing. The time mea-  
 372 surement is also used to reject cosmic muons, and to search for delayed signals. TCGs provide  
 373 triggering in the endcap regions, and consist of parallel 30  $\mu\text{m}$  wires suspended in a sensitive gas  
 374 mixture. TCGs provide high radiation tolerance and a fast response time, both features that are  
 375 necessary for handling the high flux of muons in the forward region [19].

376

377 Precision measurements of muon momentum and position are primarily achieved by MDTs.  
 378 The MDTs are constructed from 30mm diameter tubes, permeated by a gas mixture of 93% Ar and

379 7% CO<sub>2</sub>. The average single-tube spatial resolution is 80  $\mu\text{m}$ . Each chamber consists of six drift  
380 tube layers, which together provide a muon track segment resolution of 35  $\mu\text{m}$ . The momentum  
381 of the muons can be calculated from the bend in the muon trajectory as they pass through the  
382 0.5T magnetic field provided by the toroids. For a  $p_T = 1 \text{ TeV}$  track, the average  $p_T$  resolution is  
383 11%. In the inner most endcap wheels, cathode strip chambers (CSC) are used instead of MDTs,  
384 covering the region  $2.0 < |\eta| < 2.7$ . CSCs are multiwire proportional chambers, with a cathode  
385 strip readout. The CSCs have a spatial resolution in the range of 50  $\mu\text{m}$ , and a maximum drift time  
386 of about 30 ns, which makes them superior for handling the high flux of particles in the forward  
387 region [20].

### 388 3.5 Magnet System

389 The ATLAS magnet system consists of four sets of superconducting magnets: a barrel solenoid,  
390 barrel toroid, and two endcap toroids. The solenoid magnet produces a 2T magnetic field respon-  
391 sible for bending the trajectories of charged particles as they pass through the inner detector. The  
392 three toroid magnets provide a field of 0.5 - 1 T and curve the path of muons passing through the  
393 muon spectrometer.

394

395 The inner solenoid magnet is composed of over 9km of niobium-titanium superconductor  
396 wires, which are imbedded into strengthen pure aluminum strips. The solenoid is just 4.5 cm  
397 thick, which minimizes interactions between the magnet material and particles passing through the  
398 detector. It is housed in the LAr cryostat, as described in section 3.3.1, which further reduces the  
399 amount of non-detector material required to support the solenoid. The return yoke of the magnet  
400 is provided by the iron absorber of the TileCal [21].

401

402 The central ATLAS toroid magnet, providing the magnetic field for the barrel region of the MS,  
403 is the largest toroidal magnet ever constructed at 25m in length. The toroid is composed of eight  
404 individual coils, each housed in their own cryostat. The toroidal magnetic field is advantageous

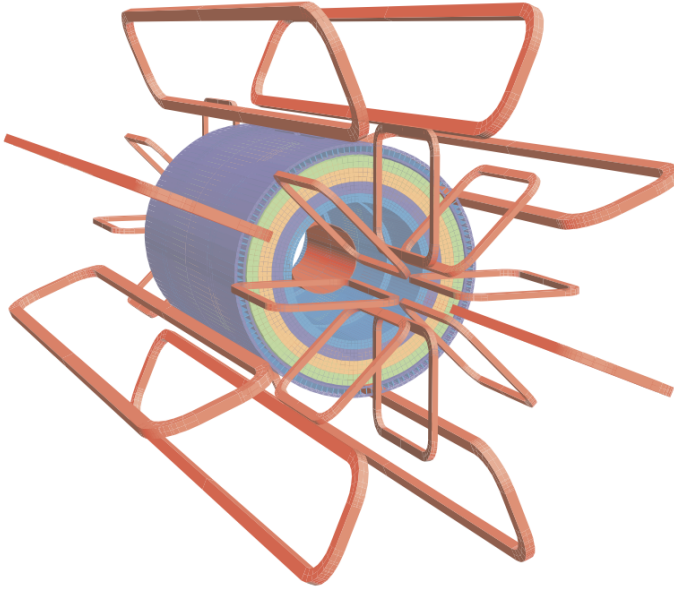


Figure 3.9: Layout of the barrel and endcap toroid magnets [22]

as the direction of the field is almost perpendicular to the path of the charged particles. 56 km of aluminum stabilized niobium-titanium-copper superconductor wire compose the magnet. In each endcap, eight smaller superconducting coils extend the toroidal magnetic field to particles leaving the detector in the forward direction [21]. Figure 3.9 shows the layout of the toroid magnets.

### 3.6 Forward Detectors

In addition to the inner detector, calorimeters, and muon spectrometer, three smaller detectors provide coverage in the very forward region. The innermost forward detector at 17 m from the interaction point is the LUminosity measurement using Cerenkov Integrating Detector (LUCID). LUCID's primary purpose is to measure the relative online-luminosity for the ATLAS detector, from inelastic  $p - p$  scattering. The detector is composed of 20 aluminum Cerenkov tubes which surround the beam pipe and face towards the interaction point. The second forward detector is the Zero-Degree Calorimeter (ZDC), located 140 m from the interaction point in both directions, at the point where the LHC beam-pipe divides into two separate pipes. The ZDC's primary purpose is to detect forward neutrons from heavy ion collisions. The third detector is the Absolute Luminosity

419 for ATLAS (ALFA) system, located 240 m from the interaction point in both directions. ALFA  
420 determines luminosity by measuring elastic scattering at small angles, from which luminosity can  
421 be calculated via the optical theorem. The detector is built from scintillating fibre trackers, which  
422 are connected to the accelerator vacuum via Roman pots, which allow the detector to come as close  
423 as 1mm to the beam without disrupting the machine vacuum. The LUCID and ALFA detectors are  
424 crucial to determining the real-time conditions of the beams and the total luminosity delivered to  
425 the ATLAS detector [22].

426 **3.7 Trigger and Data Acquisition**

427 The trigger and Data Acquisition systems (TDAQ) are responsible for selecting the most viable  
428 events to save for further downstream processing. Because of the high luminosities delivered to  
429 the ATLAS detector, not all events recorded can be saved; the 40 MHz bunch crossing rate must be  
430 reduced by 5 order of magnitude to an event storage rate of 1 kHz. The trigger system is composed  
431 of three distinct levels: level 1 (L1), level 2 (L2) and the event filter. Collectively the L2 trigger the  
432 event filter from the high level trigger (HLT).

433 The L1 trigger is implemented in the hardware of the ATLAS calorimeter and muon systems. The  
434 primary modality of the L1 trigger is to identify muons, electrons, photons, jets, and  $\tau$ -leptons  
435 with high transverse momentum. Particles with high transverse momentum are more likely to  
436 originate from direct, high energy collisions, which are most likely to produce interesting physics  
437 processes. The L1 trigger also identifies events with large missing transverse energy, which could  
438 be indicative of new physics. The L1 muon trigger (L1Muon) relies on RPC and TGC trigger  
439 chambers in the barrel and endcap regions of the muon spectrometer. The L1 calorimeter trigger  
440 (L1Calo) uses reduced granularity information collected by all the calorimeter subsystems. Results  
441 from the L1Muon and L1Calo triggers are combined by the central trigger processor (CTP), which  
442 implements a trigger ‘menu’, listing various combinations of trigger requirements. The maximum  
443 L1 acceptance rate is 75 kHz, and the L1 trigger decision must reach the front-end electronics within  
444 2.5  $\mu$ s of it’s associated bunch-crossing [22].

## Conclusion or Epilogue

446        Use this page for your epilogue or conclusion if applicable; please use only one of the titles  
447      for this page. Otherwise, you may delete it. Use this page for your epilogue or conclusion if  
448      applicable; please use only one of the titles for this page. Otherwise, you may delete it. Use this  
449      page for your epilogue or conclusion if applicable; please use only one of the titles for this page.  
450      Otherwise, you may delete it. Use this page for your epilogue or conclusion if applicable; please  
451      use only one of the titles for this page. Otherwise, you may delete it. Use this page for your  
452      epilogue or conclusion if applicable; please use only one of the titles for this page. Otherwise,  
453      you may delete it. Use this page for your epilogue or conclusion if applicable; please use only one  
454      of the titles for this page. Otherwise, you may delete it. Use this page for your epilogue or  
455      conclusion if applicable; please use only one of the titles for this page. Otherwise, you may delete  
456      it. Use this page for your epilogue or conclusion if applicable; please use only one of the titles for  
457      this page. Otherwise, you may delete it. Use this page for your epilogue or conclusion if  
458      applicable; please use only one of the titles for this page. Otherwise, you may delete it. Use this  
459      page for your epilogue or conclusion if applicable; please use only one of the titles for this page.  
460      Otherwise, you may delete it. Use this page for your epilogue or conclusion if applicable; please  
461      use only one of the titles for this page. Otherwise, you may delete it. Use this page for your  
462      epilogue or conclusion if applicable; please use only one of the titles for this page. Otherwise,  
463      you may delete it. Use this page for your epilogue or conclusion if applicable; please use only one  
464      of the titles for this page. Otherwise, you may delete it. Use this page for your epilogue or  
465      conclusion if applicable; please use only one of the titles for this page. Otherwise, you may delete

466 it. Use this page for your epilogue or conclusion if applicable; please use only one of the titles for  
467 this page. Otherwise, you may delete it. Use this page for your epilogue or conclusion if  
468 applicable; please use only one of the titles for this page. Otherwise, you may delete it. Use this  
469 page for your epilogue or conclusion if applicable; please use only one of the titles for this page.  
470 Otherwise, you may delete it. Use this page for your epilogue or conclusion if applicable; please  
471 use only one of the titles for this page. Otherwise, you may delete it. Use this page for your  
472 epilogue or conclusion if applicable; please use only one of the titles for this page. Otherwise,  
473 you may delete it. Use this page for your epilogue or conclusion if applicable; please use only one  
474 of the titles for this page. Otherwise, you may delete it. Use this page for your epilogue or  
475 conclusion if applicable; please use only one of the titles for this page. Otherwise, you may delete  
476 it. Use this page for your epilogue or conclusion if applicable; please use only one of the titles for  
477 this page. Otherwise, you may delete it. Use this page for your epilogue or conclusion if  
478 applicable; please use only one of the titles for this page. Otherwise, you may delete it. Use this  
479 page for your epilogue or conclusion if applicable; please use only one of the titles for this page.  
480 Otherwise, you may delete it. Use this page for your epilogue or conclusion if applicable; please  
481 use only one of the titles for this page. Otherwise, you may delete it. Use this page for your  
482 epilogue or conclusion if applicable; please use only one of the titles for this page. Otherwise,  
483 you may delete it. Use this page for your epilogue or conclusion if applicable; please use only one  
484 of the titles for this page. Otherwise, you may delete it. Use this page for your epilogue or  
485 conclusion if applicable; please use only one of the titles for this page. Otherwise, you may delete  
486 it. Use this page for your epilogue or conclusion if applicable; please use only one of the titles for  
487 this page. Otherwise, you may delete it. Use this page for your epilogue or conclusion if  
488 applicable; please use only one of the titles for this page. Otherwise, you may delete it. Use this  
489 page for your epilogue or conclusion if applicable; please use only one of the titles for this page.  
490 Otherwise, you may delete it. Use this page for your epilogue or conclusion if applicable; please  
491 use only one of the titles for this page. Otherwise, you may delete it. Use this page for your  
492 epilogue or conclusion if applicable; please use only one of the titles for this page. Otherwise,

493 you may delete it. Use this page for your epilogue or conclusion if applicable; please use only one  
494 of the titles for this page. Otherwise, you may delete it. Use this page for your epilogue or  
495 conclusion if applicable; please use only one of the titles for this page. Otherwise, you may delete  
496 it. Use this page for your epilogue or conclusion if applicable; please use only one of the titles for  
497 this page. Otherwise, you may delete it. Use this page for your epilogue or conclusion if  
498 applicable; please use only one of the titles for this page. Otherwise, you may delete it. Use this  
499 page for your epilogue or conclusion if applicable; please use only one of the titles for this page.  
500 Otherwise, you may delete it. Use this page for your epilogue or conclusion if applicable; please  
501 use only one of the titles for this page. Otherwise, you may delete it. Use this page for your  
502 epilogue or conclusion if applicable; please use only one of the titles for this page. Otherwise,  
503 you may delete it. Use this page for your epilogue or conclusion if applicable; please use only one  
504 of the titles for this page. Otherwise, you may delete it. Use this page for your epilogue or  
505 conclusion if applicable; please use only one of the titles for this page. Otherwise, you may delete  
506 it. Use this page for your epilogue or conclusion if applicable; please use only one of the titles for  
507 this page. Otherwise, you may delete it. Use this page for your epilogue or conclusion if  
508 applicable; please use only one of the titles for this page. Otherwise, you may delete it. Use this  
509 page for your epilogue or conclusion if applicable; please use only one of the titles for this page.  
510 Otherwise, you may delete it. Use this page for your epilogue or conclusion if applicable; please  
511 use only one of the titles for this page. Otherwise, you may delete it. Use this page for your  
512 epilogue or conclusion if applicable; please use only one of the titles for this page. Otherwise,  
513 you may delete it. Use this page for your epilogue or conclusion if applicable; please use only one  
514 of the titles for this page. Otherwise, you may delete it. Use this page for your epilogue or  
515 conclusion if applicable; please use only one of the titles for this page. Otherwise, you may delete  
516 it. Use this page for your epilogue or conclusion if applicable; please use only one of the titles for  
517 this page. Otherwise, you may delete it. Use this page for your epilogue or conclusion if  
518 applicable; please use only one of the titles for this page. Otherwise, you may delete it. Use this  
519 page for your epilogue or conclusion if applicable; please use only one of the titles for this page.

520 Otherwise, you may delete it. Use this page for your epilogue or conclusion if applicable; please  
521 use only one of the titles for this page. Otherwise, you may delete it. Use this page for your  
522 epilogue or conclusion if applicable; please use only one of the titles for this page. Otherwise,  
523 you may delete it. Use this page for your epilogue or conclusion if applicable; please use only one  
524 of the titles for this page. Otherwise, you may delete it. Use this page for your epilogue or  
525 conclusion if applicable; please use only one of the titles for this page. Otherwise, you may delete  
526 it. Use this page for your epilogue or conclusion if applicable; please use only one of the titles for  
527 this page. Otherwise, you may delete it. Use this page for your epilogue or conclusion if  
528 applicable; please use only one of the titles for this page. Otherwise, you may delete it. Use this  
529 page for your epilogue or conclusion if applicable; please use only one of the titles for this page.  
530 Otherwise, you may delete it. Use this page for your epilogue or conclusion if applicable; please  
531 use only one of the titles for this page. Otherwise, you may delete it. Use this page for your  
532 epilogue or conclusion if applicable; please use only one of the titles for this page. Otherwise,  
533 you may delete it. Use this page for your epilogue or conclusion if applicable; please use only one  
534 of the titles for this page. Otherwise, you may delete it. Use this page for your epilogue or  
535 conclusion if applicable; please use only one of the titles for this page. Otherwise, you may delete  
536 it. Use this page for your epilogue or conclusion if applicable; please use only one of the titles for  
537 this page. Otherwise, you may delete it. Use this page for your epilogue or conclusion if  
538 applicable; please use only one of the titles for this page. Otherwise, you may delete it. Use this  
539 page for your epilogue or conclusion if applicable; please use only one of the titles for this page.  
540 Otherwise, you may delete it. Use this page for your epilogue or conclusion if applicable; please  
541 use only one of the titles for this page. Otherwise, you may delete it. Use this page for your  
542 epilogue or conclusion if applicable; please use only one of the titles for this page. Otherwise,  
543 you may delete it. Use this page for your epilogue or conclusion if applicable; please use only one  
544 of the titles for this page. Otherwise, you may delete it. Use this page for your epilogue or  
545 conclusion if applicable; please use only one of the titles for this page. Otherwise, you may delete  
546 it.

## References

- [1] M. Tanabashi et al. “Review of Particle Physics”. In: *Phys. Rev. D* 98 (3 2018), pp. 847–851.
- [2] Lyndon Evans and Philip Bryant. “LHC Machine”. In: *Journal of Instrumentation* 3.08 (2008), S08001.
- [3] “The ATLAS Experiment at the CERN Large Hadron Collider”. In: *JINST* 3 (2008). Also published by CERN Geneva in 2010, S08003.
- [4] “The CMS experiment at the CERN LHC”. In: *Journal of Instrumentation* 3.08 (2008), S08004.
- [5] “The ALICE experiment at the CERN LHC”. In: *Journal of Instrumentation* 3.08 (2008), S08002.
- [6] “The LHCb Detector at the LHC”. In: *Journal of Instrumentation* 3.08 (2008), S08005.
- [7] Aad G., et al. (ATLAS Collaboration and CMS Collaboration). “Combined Measurement of the Higgs Boson Mass in pp Collisions at  $\sqrt(s) = 7$  and 8 TeV with the ATLAS and CMS Experiments”. In: *Phys. Rev. Lett.* 114 (19 2015), p. 191803.
- [8] O. Aberle et al. *High-Luminosity Large Hadron Collider (HL-LHC): Technical design report*. CERN Yellow Reports: Monographs. Geneva: CERN, 2020.
- [9] *The High-Luminosity LHC*. <https://voisins.web.cern.ch/high-luminosity-lhc-hl-lhc>. Accessed: 2024-01-05.
- [10] Ana Lopes and Melissa Loyse Perrey. *FAQ-LHC The guide*. 2022.
- [11] Esma Mobs. “The CERN accelerator complex in 2019. Complexe des accélérateurs du CERN en 2019”. In: (2019). General Photo.
- [12] *Pulling together: Super Conducting electromagnets*. <https://home.cern/science/engineering/pulling-together-superconducting-electromagnets>. Accessed: 2024-01-05.
- [13] G Aad, B Abbott, and ATLAS Collaboration. “Performance of the reconstruction of large impact parameter tracks in the inner detector of ATLAS”. In: *Eur. Phys. J. C Part. Fields* 83.11 (Nov. 2023).
- [14] Joao Pequenao. *Computer Generated image of the ATLAS calorimeter*. 2008.

- 575 [15] *ATLAS liquid-argon calorimeter: Technical Design Report*. Technical design report. AT-  
576 LAS. Geneva: CERN, 1996.
- 577 [16] H A Gordon. “Liquid argon calorimetry for the SSC”. In: () .
- 578 [17] Henric Wilkens and (on behalf ofthe ATLAS LArg Collaboration). “The ATLAS Liquid  
579 Argon calorimeter: An overview”. In: *Journal of Physics: Conference Series* 160.1 (2009),  
580 p. 012043.
- 581 [18] *Technical Design Report for the Phase-II Upgrade of the ATLAS Tile Calorimeter*. Tech.  
582 rep. Geneva: CERN, 2017.
- 583 [19] “Technical Design Report for the Phase-II Upgrade of the ATLAS Muon Spectrometer”. In:  
584 () .
- 585 [20] L Pontecorvo. “The ATLAS Muon Spectrometer”. In: (2004). revised version number 1  
586 submitted on 2003-07-27 16:31:16.
- 587 [21] *ATLAS magnet system: Technical Design Report, 1*. Technical design report. ATLAS. Geneva:  
588 CERN, 1997.
- 589 [22] The ATLAS Collaboration. “The ATLAS Experiment at the CERN Large Hadron Collider”.  
590 In: *Journal of Instrumentation* 3.08 (2008), S08003.

591

592

## **Appendix A: Experimental Equipment**

593       Lorem ipsum dolor sit amet, consectetur adipiscing elit, sed do eiusmod tempor incididunt ut  
594       labore et dolore magna aliqua. Ut enim ad minim veniam, quis nostrud exercitation ullamco laboris  
595       nisi ut aliquip ex ea commodo consequat. Duis aute irure dolor in reprehenderit in voluptate velit  
596       esse cillum dolore eu fugiat nulla pariatur. Excepteur sint occaecat cupidatat non proident, sunt in  
597       culpa qui officia deserunt mollit anim id est laborum.

## Appendix B: Data Processing

600       Lorem ipsum dolor sit amet, consectetur adipiscing elit, sed do eiusmod tempor incididunt ut  
601       labore et dolore magna aliqua. Ut enim ad minim veniam, quis nostrud exercitation ullamco laboris  
602       nisi ut aliquip ex ea commodo consequat. Duis aute irure dolor in reprehenderit in voluptate velit  
603       esse cillum dolore eu fugiat nulla pariatur. Excepteur sint occaecat cupidatat non proident, sunt in  
604       culpa qui officia deserunt mollit anim id est laborum.